Masonry structures: a proposal of analytical evaluation of fragility curves for tsunami impact - application to the Mediterranean coasts

Marco Filippo Ferrotto, Liborio Cavaleri

Department of Engineering, University of Palermo, Italy

Corresponding author details: marcofilippo.ferrotto@unipa.it, University of Palermo, Viale delle Scienze, Palermo, Italy

Abstract

Evaluation of tsunami vulnerability of coastal buildings is gaining high interest in the last years in the areas with high tsunami hazard. Fragility evaluation is a fundamental step to obtain a quantitative estimation of the probability of building damage and in order to define possible strategies for risk mitigation. Several empirical fragility curves are available for masonry structures. However, an empirical fragility curve is generally based on field surveys after tsunami events, not always available. Conversely, analytical fragility curves are based on prediction approaches. In this paper, first time, a proposal for the evaluation of analytical fragility curves for masonry structures typical of the Mediterranean coasts based on simplified structural analyses and damage indexes is presented. The proposal considers the uncertainties in the demand by the definition of the probability distribution of the inundation scenarios. Further, the uncertainties in the structural capacity are considered. Several Monte Carlo simulations on some masonry structure types have been carried out to evaluate the fragility related to each fixed damage state assuming the inundation depth as intensity measure. Comparisons with available empirical fragility curves are presented at the end of the paper.

Keywords: Tsunami loads, vulnerability, fragility curves, tsunami fragility functions, masonry structures

1. Introduction

Tsunamis are among the most dangerous and destructive events that can cause loss of humans' life and wide damage to the constructions (buildings, infrastructures, etc.). The huge loads generated by the tsunami waves make the majority of structures helpless to provide a shelter to the population during such events. Therefore, strategies for the risk mitigation such as warning, evacuation and temporary shelter in strategic structures need to be defined by a large scale analysis of the coastal areas (Unesco, 2015).

In the last decades, several earthquakes-induced tsunami events have devastated coasts causing many deaths. Among the most known there are the earthquakes in Colombian Pacific coast in 1906 and 1979 with magnitude of 8.8 and 7.6, Japan in 1993 with magnitude of 7.7, Indian Ocean in 2004 with magnitude of 9.3, Samoa in 2009 with magnitude of 8.0, Chile in 2010 with magnitude of 8.8, Japan in 2011 with magnitude of 9.0, Indonesia in 2018 with magnitude of 7.5. However, tsunamis are caused by costal or underwater landslides as well. An example is the famous Alaska tsunami in 1958.

Historically, the Mediterranean costs experienced catastrophic tsunamis: for example in 365 A.D. an earthquake with epicenter close to the Crete island was followed by a tsunami that caused 50.000 deaths along the costs of Egypt, Greece, Sicily and Palestine; in 1169, 20.000 deaths were counted along the costs around Catania because of a tsunami; in 1693 a tsunami caused over 60.000 deaths in Italy and Greece; in 1783 a tsunami caused about 2000 deaths in the Sicilian costs of Messina and Reggio Calabria; in the same costs in 1908 a tsunami caused waves up to 12 m height.

Among the structures exhibiting high vulnerability to tsunami, masonry and wood structures have revealed to be the most critical. Lower vulnerability has been observed for reinforced concrete structures and steel structures (Suppasri et al., 2013).

Fragility curves are powerful tools for the estimation of the probability of an effect (damage) related to a certain cause of which the intensity is known. Differently from the earthquakes, in which the peak ground acceleration (PGA) is assumed as intensity measure (IM), in the case of tsunami, the IM

50 can be assumed by the inundation depth or alternatively by the momentum flux, or the Froude Number
51 or again the flow velocity (Alam et al., 2018). However, most of the fragility curves are expressed in
52 function of the inundation depth (Petrone et al., 2017, Karafagka et al, 2018, Pitilakis et al., 2019,
53 Medina et al., 2019).

54 The issue of estimating fragility or vulnerability of structures subjected to earthquakes has been
55 widely analyzed in the state of the art by several authors (Lagomarsino and Giovinazzi, 2006, Silva
56 et al., 2014, Ioannou et al., 2015 Cavaleri et al., 2017, Asteris et al. 2019).

57 Empirical tsunami fragility curves are available in the literature for all types of buildings, such as
58 reinforced concrete, steel, masonry and wood (Suppasri et al., 2012, 2013, 2015, Macabuag et al.,
59 2016, 2018). These fragility curves have been proposed for the areas which experienced catastrophic
60 tsunami events. Usually, the before mentioned curves are obtained from the cumulative damage
61 probability exceedance with respect to a certain intensity measure assuming a lognormal distribution
62 of the data, but other approaches have also been proposed (Charvet et al. 2017).

63 Conversely, analytical fragility curves have been proposed mainly for reinforced concrete and steel
64 moment resisting frame structures (Foytong et al., 2015, Petrone et al., 2017, Karafagka et al, 2018,
65 Medina et al., 2019). On the best knowledge of the authors, no analytical fragility functions for
66 masonry buildings have been proposed until now.

67 In this paper, a proposal for the evaluation of analytical fragility curves for masonry structures typical
68 of Mediterranean coasts based on local analyses and local damage indexes is presented. The proposal
69 considers the various uncertainties in the load demand by the definition of different scenarios and the
70 uncertainties in the structural capacity. The fragility related to each fixed damage state is represented
71 assuming the inundation depth as tsunami intensity measure. Comparisons with available empirical
72 fragility curves are presented at the end of the paper.

73

2. Proposed methodology

2.1 Fragility curves

Fragility functions are cumulative distribution functions that represent the probability of exceedance of a certain damage state for a given type of building over a range of values of tsunami intensity. In the present study, a log-normal distribution function is assumed for the evaluation of the fragility for each damage state.

$$P[DSi, IM] = \phi\left(\frac{\ln(IM) - \ln(\overline{IM})}{\beta}\right) \quad (1)$$

$$\beta = \sqrt{\beta_C^2 + \beta_D^2} \quad (2)$$

where, ϕ is the standard normal cumulative distribution function, IM is the intensity measure of the tsunami (in this case the inundation depth), $\overline{IM}$ refers to a median value and β is the log-standard deviation of the building fragilities for each damage state *DSi* depending on a certain demand parameter assumed as a control variable for the damage state.

The parameter β accounts for the uncertainties in the capacity β_C and uncertainties in the demand β_D and is expressed as the square root of the sum of the squares of the two deviation components (Karafagka et al., 2018). In turn, the log-standard deviation of the capacity is evaluated from the capacity of each structural response considering the uncertainties (see next section), while the log-standard deviation of the demand is evaluated from the difference between the polynomial function fitting the logarithms EDP-IM (Engineering Demand Parameters – Intensity Measure) with respect to the EDP-IM pairs obtained from a Monte Carlo simulation.

2.1.1 Uncertainties

Several approaches for the consideration of uncertainties have been used since there is not a standard methodology available in the state of the art. For example, Karafagka et al. (2018) assumed statistically independent uncertainties of the demand and the capacity. For the latter, they fixed the

uncertainties for low-code buildings by a value of 0.3 according to HAZUS-MH guidelines and evaluated the uncertainties in the demand by regression analysis of the results obtained by non-linear static time-history analyses. Medina, et al. (2019) evaluated the uncertainties in the results of the analyses performed after the definition of stochastic parameters for the tsunami forces and the capacity models.

In the present study, the uncertainties were defined for: i) the geometry of the building by auniform distribution, ii) the material properties by a Gaussian distribution and iii) the tsunami loads by a uniform distribution.

2.1.2 Procedure flowchart for fragility curves

The evaluation of the fragility curves starts from the definition of an inundation depth range. Random values for the flow velocity are assumed for the evaluation of the hydrodynamic and impulsive forces that depend also on the breadth of the construction in the direction orthogonal to the flow B and the opening coefficient C_O (randomly defined) as well as the hydrostatic component. The other involved geometrical variables are the interstory height H, the length of the walls subjected to in-plane actions L, the wall thickness t. Therefore, pressure distribution on the structural walls are obtained depending on the inundation depth h. Then, in-plane and out-of-plane forces (bending moment, shear) are obtained from two cases of actions that are provided i) by the hydrostatic and hydrodynamic component and ii) by the impulsive component. Maximum actions are assumed among the two cases for the subsequent determination of the capacity, considering uniform randomly distributed thickness of the walls and normal distribution of the mechanical characteristics of the masonry such as the compressive and shear strengths. Subsequently, regression analysis of the demand (logarithm of inundation depth – EDP pairs) is performed for each capacity model and the median values of inundation depth for a given damage state (capacity) are obtained. Then, fragility curves are obtained

considering the log-standard deviation of the demand and the capacity for each damage state considered.

The flowchart for the evaluation of the fragility curves is shown in Fig. 1.

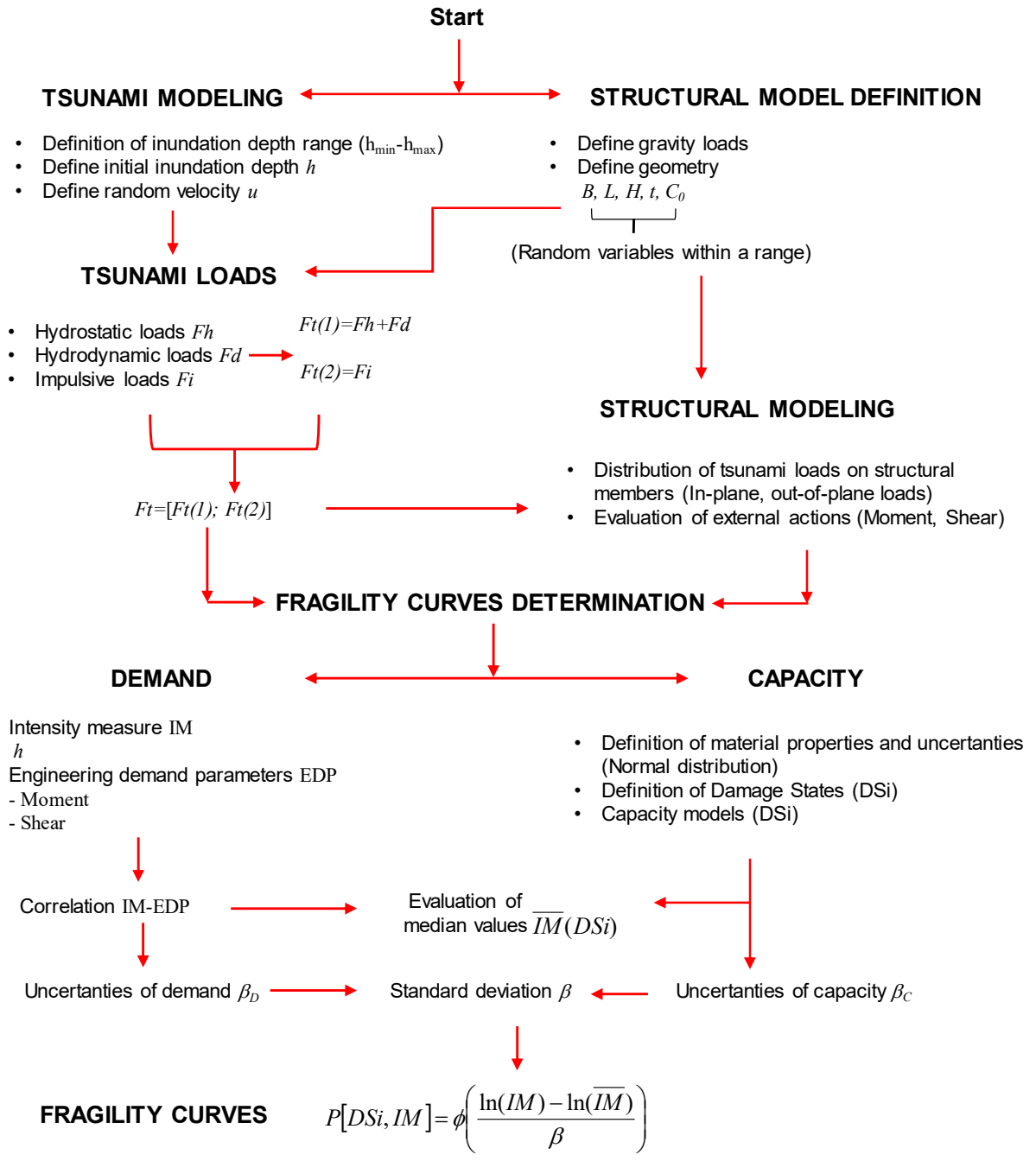

Fig. 1. Flowchart for the process of definition of fragility curves.

125 **2.2 Tsunami loads**

126 In the analytical evaluation of tsunami fragility, the definition of tsunami forces acting on buildings
127 is basic. According to standard code as ASCE/SEI 7-16 and FEMA P646, a tsunami wave against an
128 obstacle generates different forces including the impact, the hydrodynamic component, the impact of
129 debris and the debris damming. In addition, buoyancy and uplift forces should be considered as well
130 as water retained at elevated floors.

131 These forces occur not at the same time, however, the above standard codes suggest how to combine
132 tsunami forces to be applied to the overall structure and to individual structural components. Other
133 studies provided an analytical formulation for the definition of the hydrodynamic forces by equations
134 validated by experimental testing (Triatmadja et al., 2012, Robertson et al., 2013, Qi et al., 2014,
135 Shafiei et al., 2016, Foster et al., 2017, Wüthrich et al., 2018 a, b, c,). From the available studies, high
136 variability in the resulting forces is observed since the analytical models are affected by high scatter.
137 The problem is mainly related to the estimation of the flow velocity that causes, for a given inundation
138 depth, a wide range of possible tsunami forces.

139 In the present study, it is proposed to evaluate the tsunami forces according to FEMA P646,
140 considering the total force as a sum of the hydrostatic and the hydrodynamic forces resulting from a
141 given inundation depth and flow velocity as expressed in the following equations:

$$Fh = 0.5 B C_O \rho g h^2 \tag{3a}$$

$$Fd = 0.5 B \rho C_O C_D (h u^2) \tag{3b}$$

142 In Eq. 3 Fh and Fd the hydrostatic and hydrodynamic forces, B the breadth of the building in the
143 direction orthogonal to the flow (as before mentioned), ρ is the fluid density including sediments
144 (assumed 1100 kg/m^3), g is the gravitational acceleration, h the inundation depth, C_D is the drag
145 coefficient, C_O the opening coefficient and (hu^2) the momentum flux. The maximum flow velocity u
146 and the maximum momentum flux (hu^2) are estimated by the following equations for a given range
147 of the parameter k according to Medina et al. (2019):

$$u_{\max} = k\sqrt{2gR\left(1-\frac{z}{R}\right)},\ k_{\max} = 0.7 \tag{4}$$

$$\left(hu^2\right)_{\max} = gR^2\left(0.125 - 0.235\frac{z}{R} + 0.11\left(\frac{z}{R}\right)^2\right) \tag{5}$$

148 In Eq. (5) R is the Run-up height and *z* is the ground elevation of the construction with respect to the
149 sea level.

150 In addition, at the moment of impact with the structure, impulsive forces need to be evaluated. FEMA
151 P646 estimates the impulsive force *Fi* by 1.5 times the hydrodynamic force. However, as assumed
152 also by Medina et al. 2019, this coefficient can vary between 1 and 1.5 depending on the orientation
153 of the structure with respect to the direction of the tsunami flow. Therefore, a variable multiplying
154 parameter is assumed in this study:

$$Fi = \alpha\, Fd, \qquad 1 \le \alpha \le 1.5 \tag{6}$$

155 In this study, as will be explained in the section related to the uncertainties, the flow velocity is
156 assumed as stochastic variable as well as the impulsive coefficient α , the opening coefficient, the
157 breadth of the construction orthogonal to the direction of the tsunami flow *B* and the flow velocity *u*.

158 The present approach, as well as other studies, neglects the contribution of debris impact and debris
159 damming effects because of the high variability in the evaluation of these forces. Moreover, scouring
160 effects and buoyancy are not considered.

161 **2.3 Damage states**

162 For the analytical evaluation of tsunami fragility, there are different approaches available in the state
163 of the literature that consider a global damage index and local damage indexes as the interstorey drift
164 ratio or coupled effects of maximum deformation and hysteretic energy (Petrone et al., 2017, Medina
165 et al., 2019) or damage state based on local strain (Karafagka et al., 2018). It is worth noting that
166 these approaches were used for analytical evaluation of tsunami fragility for reinforced concrete

167 structures. On the best knowledge of the authors, no analytical fragility functions are available for
168 masonry structures.

169 Other approaches are available from empirical fragility evaluation. The damage states defined by
170 Suppasri et al. (2013, 2015) relates the building conditions at the end of the tsunami inundation with
171 a specific index for different damage states, from non-structural damage, slight damage, medium
172 damage, extensive damage, collapse or washed away. However, the definition of proper damage
173 states for analytical fragility evaluation is a real challenge because it is not easy to relate a particular
174 failure condition of a certain structural member to a specific damage especially in the case of
175 nonstructural damage.

176 In this study, it is proposed to associate the collapse state to the reaching of the capacity of the
177 members evaluated by local approach, while the intermediate states are empirically assumed as a
178 percentage of the ultimate conditions. In details, non-structural damage is not considered in the
179 present study, while slight damage (DS2), moderate damage (DS3) and extensive damage (DS4) have
180 been defined as the 10%, 40% and the 70% of the ultimate conditions defined by the collapse (DS5).
181 These assumptions derived from calibration and comparisons with empirical fragility curves
182 proposed by Reese et al. (2011), Suppasri et al. (2015) and Dias et al. (2019) for single storey masonry
183 structures. Details will be shown in the section related to the results.

184

185 **2.4 Structural modeling and capacity models for building typologies**

186 The behavior of a structural type of masonry building subjected to tsunami loads has been identified
187 through a series of geometric and structural considerations that depend on the construction techniques
188 of the area as well as on the static scheme.

189 Considering a structural modeling approach based on local analysis and local damage, buildings with
190 significantly different dimensions can have a similar response according to the static scheme. In the
191 present work, the structural schemes have been identified according to Fig. 2 and Fig 3. Buildings

192 with regular and non-regular plan have been assessed belonging to the same typology considering the
193 area of influence affecting the walls in the direction of impact of the tsunami waves.

194 The aim of the study is to propose a simple approach by simplified analysis schemes for which no
195 particular software implementation is required and the solution can be obtained by fast and simple
196 computational methods.

197 *2.4.1 Out-of-plane behavior*

198 Regarding the out-of-plane behavior, the structure internal forces are evaluated by applying the loads
199 considering the area exposed to the tsunami waves according to the scheme shown in Fig. 2. Vertical
200 and horizontal bending moment at collapse were considered. The out-of-plane vertical bending
201 moment mechanism is manifested by the formation of hinges in correspondence to the maximum
202 moment in presence of a given axial load. The capacity $M_{\max} - OOP_v$ was evaluated according to the
203 current Italian Building Code 2018 by means of the following equation.

$$M_{\max} - OOP_v = \left(C_O \cdot t^2 \cdot B \cdot \frac{\sigma_0}{2} \right) \left(1 - \frac{\sigma_0}{0.85 f_m} \right) \tag{7}$$

204 being σ_0 the compressive stress acting on the cross-section, f_m the compressive strength, t the
205 thickness, C_O the opening coefficient and B the breadth of the masonry wall exposed to the tsunami
206 wave.

207 The horizontal out-of-plane bending capacity is evaluated by considering the arch effect of the
208 masonry walls. The mechanism is manifested by the expulsion of material from the top area of the
209 wall and the detachment of wedge-shaped bodies accompanied by the formation of oblique and
210 vertical plastic hinges. It is the particular case in which the activation of the kinematic mechanism is
211 due to the crushing of the masonry at the plastic hinges.

$$M_{\max} - OOP_h = f_m \cdot C_O \cdot H \cdot \frac{t}{2} \cdot f; \qquad f = \frac{t}{3} \tag{8}$$

In Eq. (8), H is the height of the masonry wall, and f defines the position of the resultant of the internal forces at the ends cross-sections (Fig. 2). Note that, due to the assumption of a certain percentage of opening in the walls, to consider a reduced resisting area, the opening coefficient has been assigned in the evaluation of the capacity. Further, an opening coefficient has been adopted in the evaluation of the tsunami forces. These two coefficient may be different.

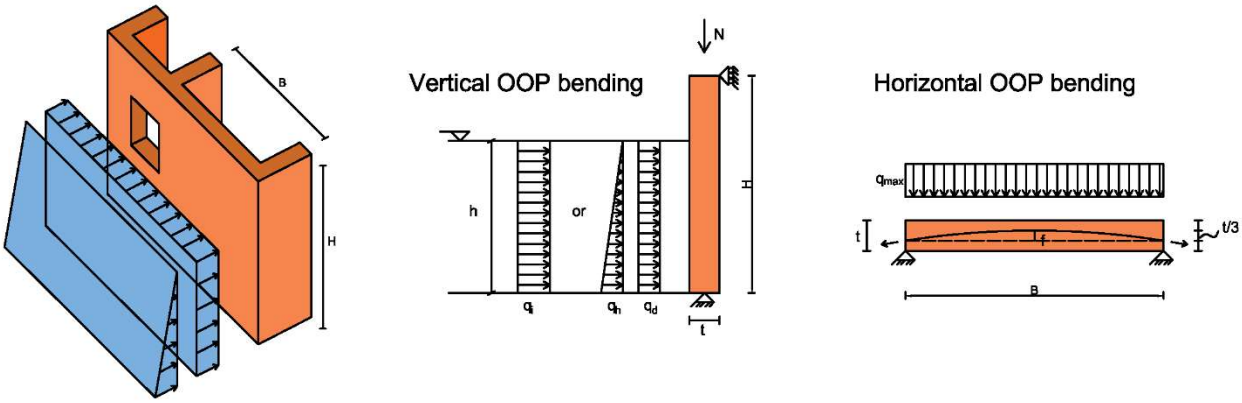

Fig. 2. Analysis scheme of the evaluation of the out-of-plane behavior

2.4.2 In-plane behavior

The in-plane behavior is considered by the evaluation of the in-plane bending moment and shear obtained according to the scheme shown in Fig. 3. Given the pressure induced by the wave on the walls encountered out-of-plane (see again Fig. 3), it is possible to evaluate the in-plane shear and the in-plane bending moment in the walls not directly hit by water. The extension of the walls is identified by the openings. Differently from the case of seismic analysis with forces applied as concentrated loads at floor level, in the case of tsunami forces, the application point of the tsunami loads depends on the inundation depth and the distribution of the forces cannot be done depending only by the stiffness of the walls. According to the scheme of Fig. 3, given two walls separated by a hole, it has been observed that the majority of shear forces are absorbed by the first wall (*bsx*) and the shear

contribution in the second wall (*bdx*) are often negligible. Numerical parametric analyses were performed for different configuration of i) ratio between *bsx* and *bdx* (from 0.25 to 2), and ii) ratio between the application point of the tsunami load *c* and the wall height *H* ($0.3 \leq c/H \leq 1$). The results are shown in Fig. 4 a, indicating the ratio between the shear force absorbed by the first wall and the second wall and the external tsunami forces depending on the application point for different dimension of the walls. In Fig. 4 b the ratio between the shear force absorbed by the first wall and the external forces is expressed depending on the ratio between the first and the second wall *bsx*/*bdx*. Based on these results, a simple empirical equation for the shear coefficient *cs* is proposed for the evaluation of the shear force to be applied to the first wall without the need to calculate shear and flexural stiffness of the walls. The equation is expressed depending on the ratio between the inundation depth *h* and the height of the walls *H*.

$$cs = 1 + \frac{bsx}{bdx}\left(0.255\left(\frac{h}{H}\right) - 0.144\right) - 0.19\left(\frac{h}{H}\right) - 0.081\left(\frac{h}{H}\right)^2 \tag{9}$$

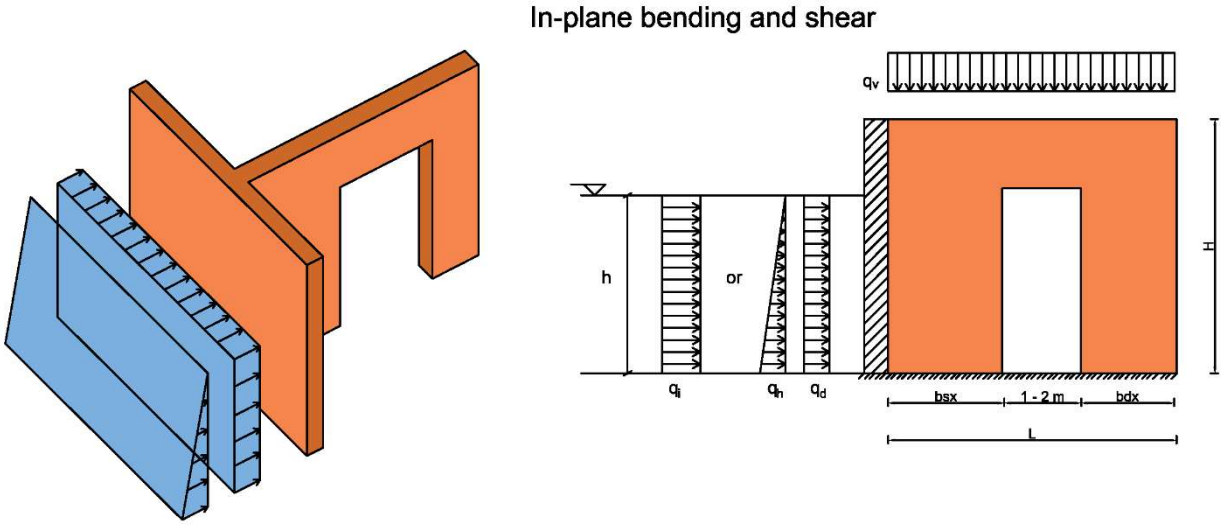

Fig. 3. Analysis scheme of the evaluation of the in-plane behavior

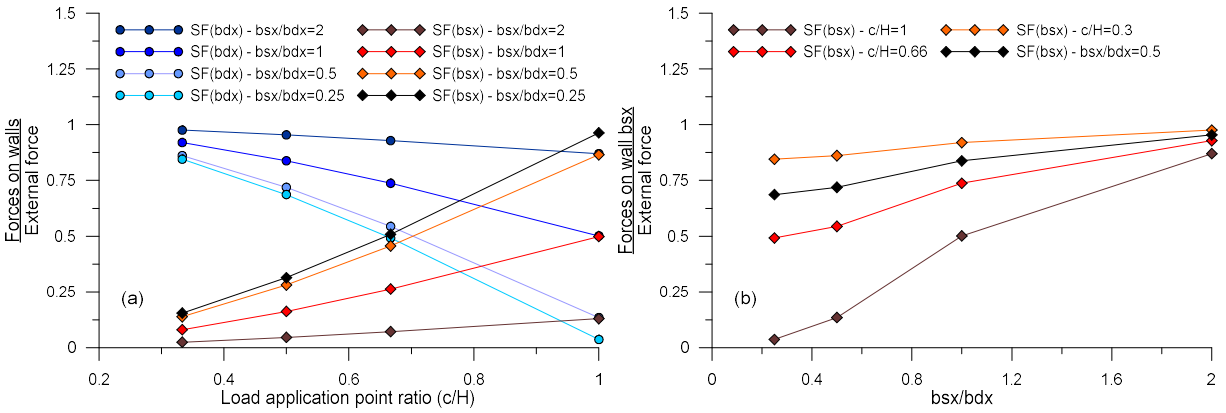

Fig. 4. Ratio between shear in-plane force on walls and the external force for different application load points and dimensions.

The maximum bending moment and shear obtained from the analysis model were compared with the capacity by means of the equation proposed by the Italian Building Code 2018 for the moment and the shear as follows:

$$M_{\max} - IP_v = \left(C_O \cdot L^2 \cdot t \cdot \frac{\sigma_0}{2} \right) \left(1 - \frac{\sigma_0}{0.85 f_m} \right) \tag{10}$$

$$V_t = C_O \cdot L \cdot t \cdot \frac{1.5\tau_0}{b} \sqrt{1 + \frac{\sigma_0}{1.5\tau_0}} \tag{11}$$

Eq. (10) represents the bending moment capacity for a given axial load. Eq. (11) expresses the shear capacity related to the diagonal shear failure provided by the Turnsek-Cacovic failure criterion, in which τ_0 is the average tangential strength. Italian Building Code 2018 provides a specific range of τ_0 for each masonry typology.

3. Application of the proposed procedure to a study area

3.1 Description of the site and identification of the structural typologies

Masonry structure buildings are the most diffused structural typology in the Mediterranean area. This is true as in the hinterland as in the coast. Recently, the Italian National Institute of Geophysics and Volcanology (INGV Italy) carried out a tsunami hazard analysis of the Mediterranean coasts,

261 selecting 47 points of interest around the coast and providing onshore and offshore tsunami hazard
262 curves for an exposure time of 50 years. It was found a high variability of possible values of maximum
263 inundation heights (MIH) depending on a probability of exceedance (PoE) in a range of 10^{-6}-10^{0}. In
264 detail, the range of MIH covers values up to 26 meters (PoE=10^{-6}); assuming a tsunami return period
265 of 2500 years (tsunami return period can range over 2000 or more years – Rubin et al. 2017), the
266 maximum inundation heights range is between 0.6 and 6.4 m (lowest MIH values related to the points
267 of study in the North-West coast, higher values related to the South-East coast). These inundation
268 depths cause very dangerous events for constructions, considering that tsunami having these
269 characteristics are destructive for most of buildings, especially those having high vulnerability to
270 seismic events. For these areas, it is important to assess adequate strategies for risk mitigation
271 especially for sites experiencing high density of population. The kilometers of coast of the East-South
272 Sicily are also of high impact in terms of number of tourists in a year. The touristic interest in the area
273 of the Siracusa (famous for the ancient Greek settlement) or Ragusa (famous for the baroque
274 monuments) increases the people flow. One of the typical costal summer destinations is for example
275 Marzamemi, a small fishing village (about 400 people). The village is almost all surrounded by the
276 Ionian Sea and the level is lower than the sea (Fig. 5). In the summer, its population increases
277 considerably (more than 20 times), due to the numerous influx of tourism, coming also from foreign
278 countries.

279 The historic center is mainly constituted by old masonry buildings. A number of reinforced concrete
280 buildings is also present but they are out of the scope of this work. The masonry constructions
281 considered in the present study are simple constructions of one, two or at most three elevations, with
282 wooden or reinforced concrete slabs (Fig. 6). Historic masonry buildings are also present including
283 churches and the old tuna market. Limestone masonry has been identified as the main construction
284 material and the structures present poor effectiveness of the joints because the buildings belong to a
285 period in which the technical codes did not follow specific seismic details in the design. Field surveys

were carried out to reach an adequate level of knowledge to identify building typologies for large scale analysis.

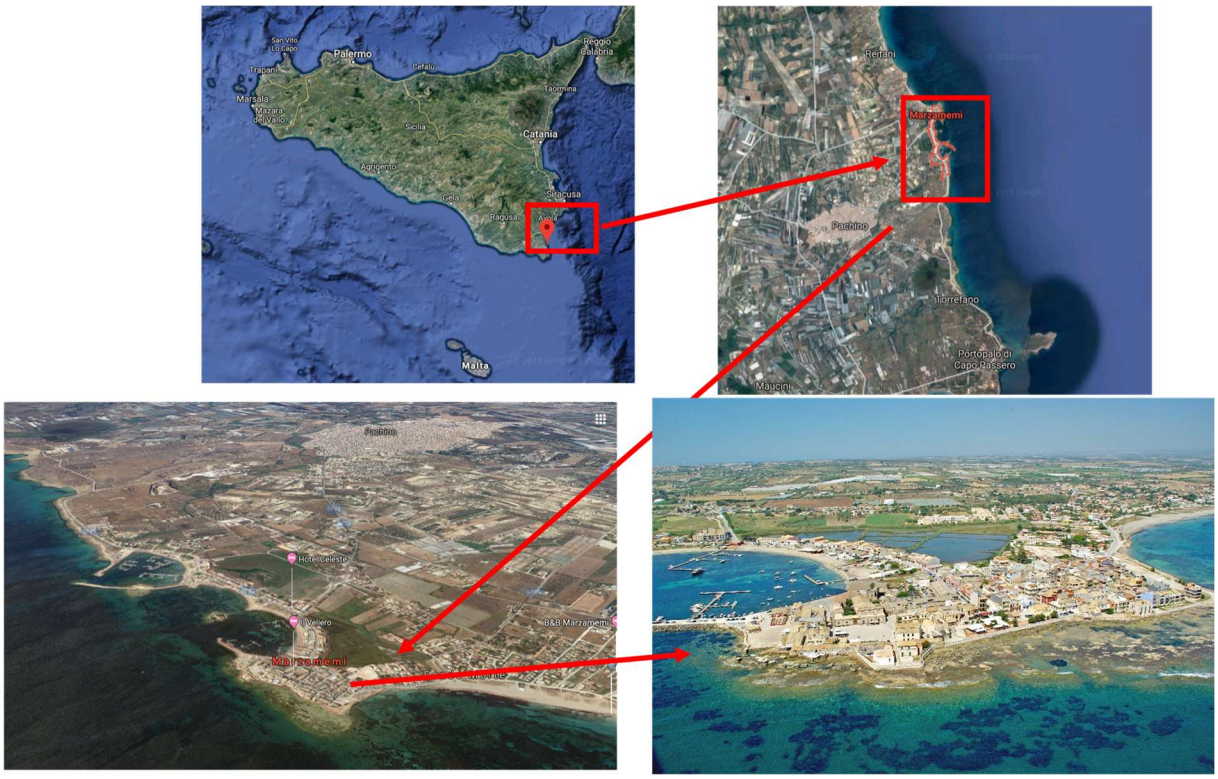

Fig. 5. Marzamemi, Sicily

Fig. 6. Typical masonry buildings in the old center of Marzamemi.

293 Based on the above considerations, three structural typologies were identified. The typology M1,
294 consisting of small single-elevation masonry buildings used as residential buildings and medium-
295 sized buildings for commercial use, with wooden floors (flat or sloping roofs) and interstory height
296 of 4-6 meters. This type belongs to ancient buildings that are used by residents or have been adapted
297 to provide accommodation for tourists or for commercial activities.

298 The M2 type, consisting of small brick residential buildings with one elevation more recent than the
299 M1 type and having reinforced concrete slabs and interstory height of 3-4 meters. Finally, the M3
300 type, consisting of residential masonry buildings with two or more stories and reinforced concrete
301 slabs and interstory height of 3-4 meters. No particular differences were observed in the response of
302 buildings with two or three floors, therefore they were grouped in the same typology. The typologies
303 classification is schematized in Fig. 7.

304 The capacity models defined for the evaluation of the structural member response under tsunami
305 loads have been identified by the in-plane and out-of-plane behavior with respect to the shear and the
306 flexural capacity.

307

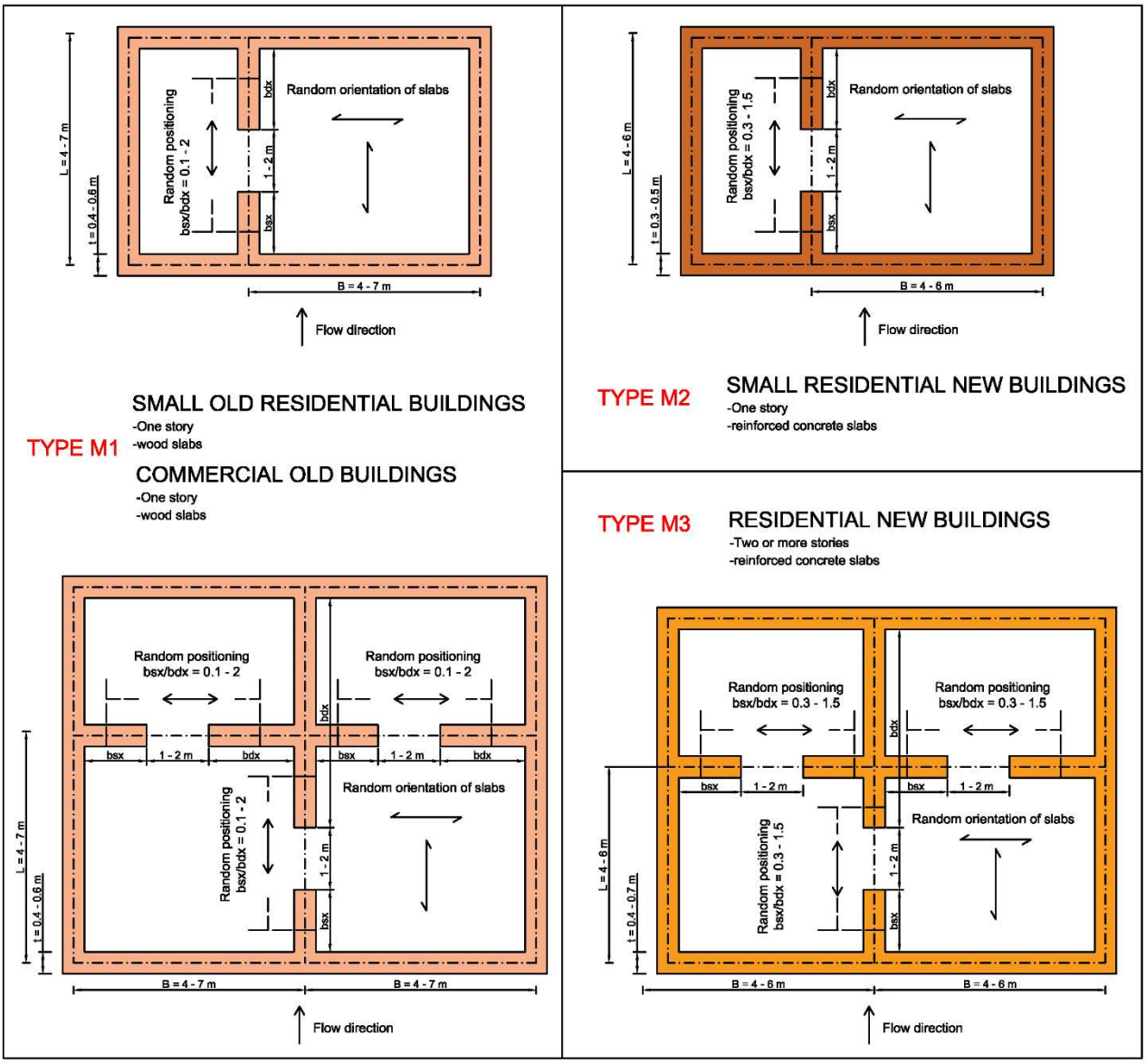

Fig. 7. Masonry building typologies.

3.2 Application of the proposed procedure

The aim of adopting probabilistic scenarios both for the determination of random excitations and the evaluation of the structural capacity is a common and efficient approach used by several authors (Benfratello et al., 2009, Cavaleri and Papia, 2014, Medina et al., 2019).

The proposed procedure described in section 2 is based on a Monte Carlo simulation with random input, random structural geometry and random mechanical characteristics of the materials. Random

317 variables are generated within a specific range as shown in Tab. 1. Random values have been
318 generated consistently with the probabilistic distribution assigned. In detail, regarding the geometry
319 defined according to the results of the surveys and the classification of the typologies as shown in
320 Fig. 7, ranges of the values for the parameters B, L, t and the opening coefficient C_O have been fixed.
321 For the mechanical properties of the masonry, low and medium masonry strength class were defined
322 for M1 and M2-M3 typologies respectively. Mean and standard deviation values for compressive and
323 shear strength have been fixed basing on the provisions of the Italian Building Code 2018 (a Gaussian
324 distribution has been supposed). Finally, random values for the flow velocity u and the impact
325 coefficient α have been generated, having assumed a uniform distribution for these parameters.

326 Inundation depth range has been defined from 1 m to 4 m assuming increase intervals of 0.5 m. For
327 each value of inundation depth h, random values of the flow velocity and the momentum flux were
328 generated so that, for a given value of inundation depth, a number of different tsunami loads were
329 calculated. Tsunami loads (hydrostatic, hydrodynamic and impulsive components) were also
330 influenced by the variables B and C_O (Eqs. 3a and 3b). For the in-plane actions, tsunami loads were
331 calculated depending on the area of influence and then they were distributed to the walls parallel to
332 the tsunami flow according to the scheme in Fig. 3 by means of Eq. 9. In this step, the presence of
333 openings on the walls were considered assuming the values of the width: 1 m, 1.5 m or 2 m.

334 For each analysis case, depending on the thickness t of the walls and the compressive and shear
335 strength of the masonry, the capacity (collapse damage state) was calculated by Eqs. 7-8 and 10-11
336 (results shown in Fig. 8).

337 For each action, regression analysis of the logarithm of inundation depth – EDP pairs allowed the
338 definition of polynomial fitting laws that were used for the calculation of the inundation depths related
339 to the collapse damage state for a given capacity (Fig 9). Then, it was possible to evaluate the median
340 values. At this point, log-standard deviations of the demand (β_D) were evaluated calculating the
341 dispersion of the logarithms of inundation depth - EDP simulated data with respect to the regression

342 fit according to Karafagka et al. (2018), while the log-standard deviations of the capacity (β_C) (for
343 each capacity associated to the collapse state and therefore depending on the median values of
344 $h_{M_{\max-OOP_v}}$, $h_{M_{\max-OOP_h}}$, $h_{M_{\max-IP}}$, h_{V_t}) were determined based on the dispersion of the results themselves
345 (Fig. 10).

346 For the intermediate damage states (slight, moderate, extensive) the same procedure was applied,
347 evaluating the capacities as a percentage of that obtained at collapse.

348

349 **Table 1. Uncertainties assumed for the definition of the fragility curves**

Properties	Variables	Range/mean/standard deviation	Distribution
Geometry	*B, L, t*	4 m-7 m, 4 m-7 m, 0.4 m-0.6 m - (M1) 4 m -6 m, 4 m -6 m, 0.3 m-0.5 m - (M2) 4 m-6 m, 4 m-6 m, 0.4 m-0.7 m - (M3)	Uniform
	Opening coefficient C_O	0.5-1	
Materials	f_m	1.8 MPa (mean); ±0.8 MPa (standard deviation) - (M1) 2.3 MPa (mean) ± 0.9 MPa (standard deviation) - (M2-M3)	Gaussian
	τ_0	0.037 MPa (mean) ± 0.019 MPa (standard deviation) - (M1) 0.054 MPa (mean) ± 0.026 MPa (standard deviation) - (M2-M3)	
Tsunami loads	Flow velocity u	$u = 0.7u_{\max} \div u_{\max}$	Uniform
	Impact coefficient α	1 - 1.5	

350

351

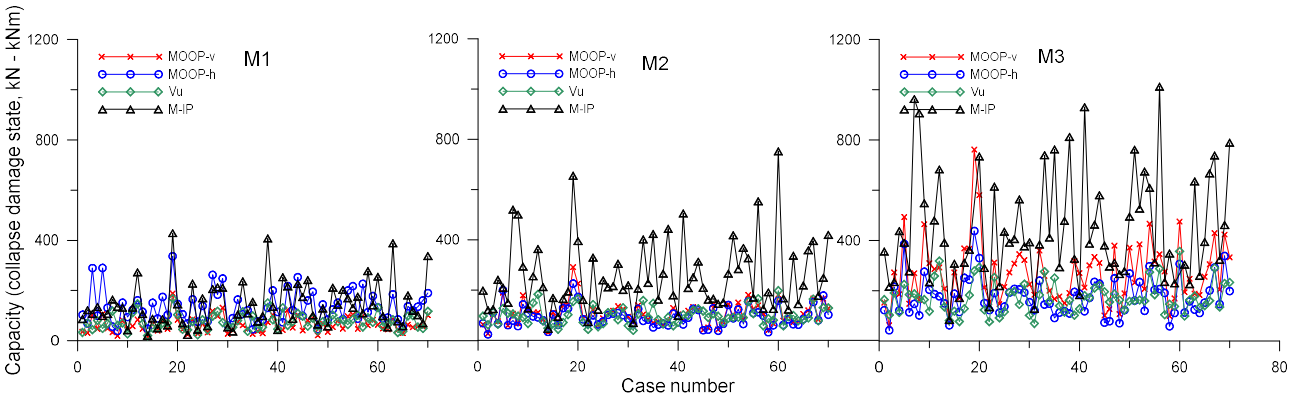

352

353 **Fig. 8. Capacity values obtained from different analysis cases**

354

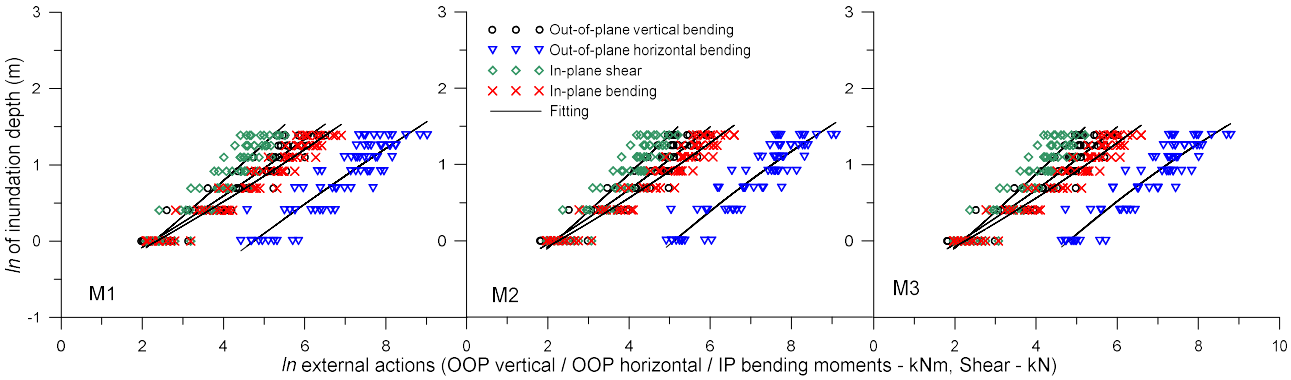

355

356 **Fig. 9. *Logarithm of* inundation depth-external actions pairs**

357

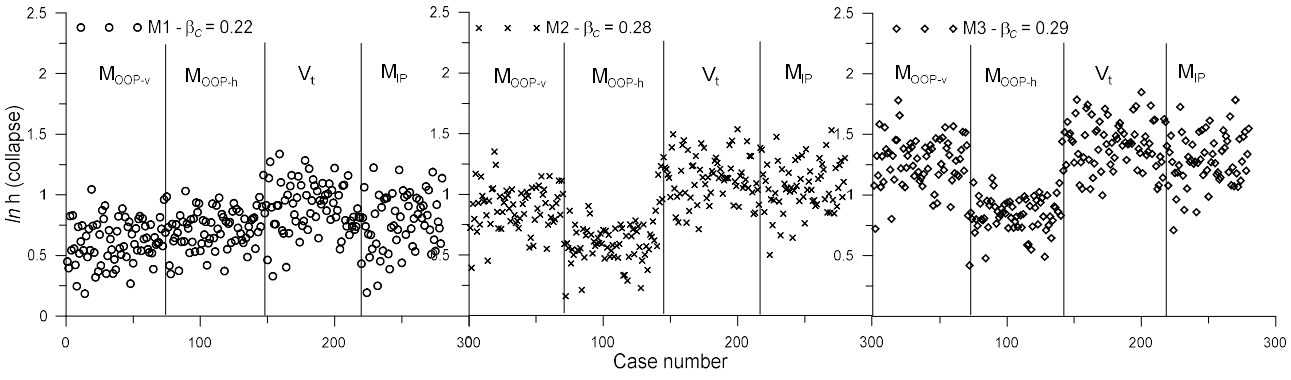

358

359 **Fig. 10. *Logarithm of* inundation depth at collapse state.**

360

4. Fragility curves

In this section the results of the above analysis are presented for the masonry building typologies defined for the study area around Marzamemi. Comparisons in terms of fragility at collapse state for the three typologies of buildings are shown in Fig. 11a. For these building typologies, the median values of inundation depth at collapse damage state resulted 2.11 m, 2.52 and 3.35 for buildings M1, M2 and M3 respectively. These fragility curves were obtained with a log-standard deviation β of 0.27, 0.32 and 0.34.

The consistency in the results can be observed by the differences between the higher fragility expressed by the masonry type M1 with respect to the masonry type M2. Although the M1 type has walls with a thickness greater than that of the M2 type (0.4 m - 0.6 m against 0.3 m - 0.5 m), the higher mechanical characteristics of the masonry compensates for its performances. In addition, the reduced lengths of the walls exposed to the tsunami actions reduce the tsunami forces as they are related to the exposure of the building to the wave. Another substantial difference in the capacity is due to the differences in the dimensionless external axial load acting on the walls. M1 type buildings, with wooden floors, have lower dimensionless compressive stress levels compared to buildings with reinforced concrete slabs which (around 0.1 for M1 compared with around 0.2 for M2). This effect is more important in the case of buildings type M3, in which although the thicknesses is slightly higher, the normal stress level still increases (about 0.35), influencing positively their capacity. In fact, masonry buildings with two or more storey resulted much stronger (lower vulnerable) with respect to single-storey masonry at the same inundation depth. These achievements are in accordance with empirical observations available in the literature (Suppasri et al. 2015).

In Fig 11 b, c, d the fragility curves obtained for the four damage state considered are shown for all the masonry types. For the extensive damage state, the median values of inundation depth resulted 1.84 m, 2.16 and 2.88 m for the typologies M1, M2 and M3 respectively. For the moderate damage

state, these values resulted 1.49 m, 1.71 m and 1.27 m, while for the slight damage state the median values resulted 0.89 m, 0.97 m and 1.27 m for M1, M2 and M3 respectively.

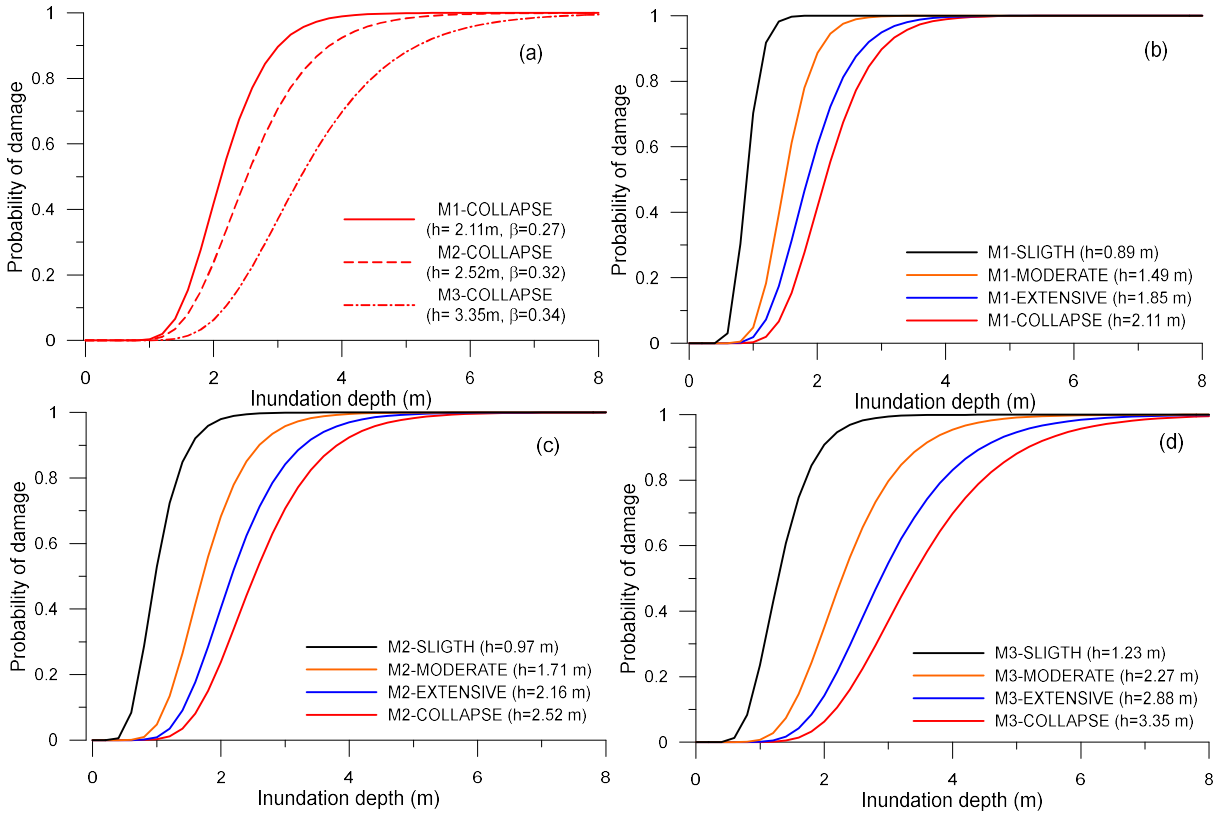

Fig. 11. Fragility curves for the building typologies of Marzamemi. Comparisons at collapse state (a); Fragility at different damage state for single-storey masonry type M1 (b) and M2 (c) and multi-storey masonry type M3 (d)

The comparisons of the analytical fragility curves obtained in the present study for single-storey masonry buildings (for building typologies M1 and M2) for all the damage states are compared with empirical ones available in the literature. The empirical fragility curves considered for comparisons are those obtained by Reese et al. (2011), Suppasri et al. (2015) and Dias et al. (2019). The comparisons are shown in Fig. 12 a-d, showing a good agreement between the fragility curves proposed in the present study and those proposed by the above authors, being the proposed analytical fragility curves within a range between the curves coming from the studies in question.

It can be considered a good goal due to the fact that the nature of the curves is different because they are obtained from different approaches and procedures. In detail, Reese et al. (2011) obtained fragility

curves from American Samoa and Samoa (formerly Western Samoa) sites after the 2009 South Pacific tsunami. The authors carried out field surveys on twelve villages on more than 200 buildings, among which the majority were masonry residential buildings (120 buildings). The authors do not give particular information on the dimensions of the buildings, nor on the type of materials and construction techniques adopted but classify the buildings simply as masonry buildings. The authors used logistic regression to derive fragility curves for five damage states (DS1 to DS5 for Light, Minor, Moderate, Severe and Collapse damage states respectively) and obtained median and log-standard deviation values of 0.46 m and 0.40 for DS2, 1.28 m and 0.35 for DS3, 1.86 m and 0.41 for DS4, and 2.49 m and 0.40 for DS5. These values are in agreement with those proposed in the present study obtained by analytical procedure.

Suppasri et al. (2015) obtained fragility curves based on data from the 2011 Tohoku-Oki Tsunami in Ishinomaki City. The authors used regression analysis on log-normal distribution of data to characterize fragility curves based on damage date collected by the Ministry of Land, Infrastructure, and Transport (MLIT), defining 6 different damage from LV1 to LV6 to identify Minor Damage, Moderate Damage, Major Damage, Complete Damage, Collapsed and Washed Away. The authors provided also a discussion of the parameters influencing building damage depending on structural material and number of stories, building function and construction year. However, no information on the geometry and the dimensions was provided. In the present study, single-storey residential and commercial building types were considered for comparisons. Results are close to that provided by the proposed analytical procedure (see Fig. 12).

Finally, Dias et al. (2019) proposed fragility curves for four damage states for masonry buildings based on the studies of Reese et al. (2011) and Nanayakkara and Dias (2013, 2016). The authors assumed DS1 as non-structural damage state (therefore it was not included for the comparisons in the present study), DS2 and DS3 as Moderate and Heavy Structural damage states (with median values of inundation depth of 0.87 m and 1.86 m respectively) and DS4 as Collapse damage state (with

median values of inundation depth of 2.49 m). As stated above for the other studies, also in this case there is a good consistency between the empirical fragility curves and the proposed analytical ones.

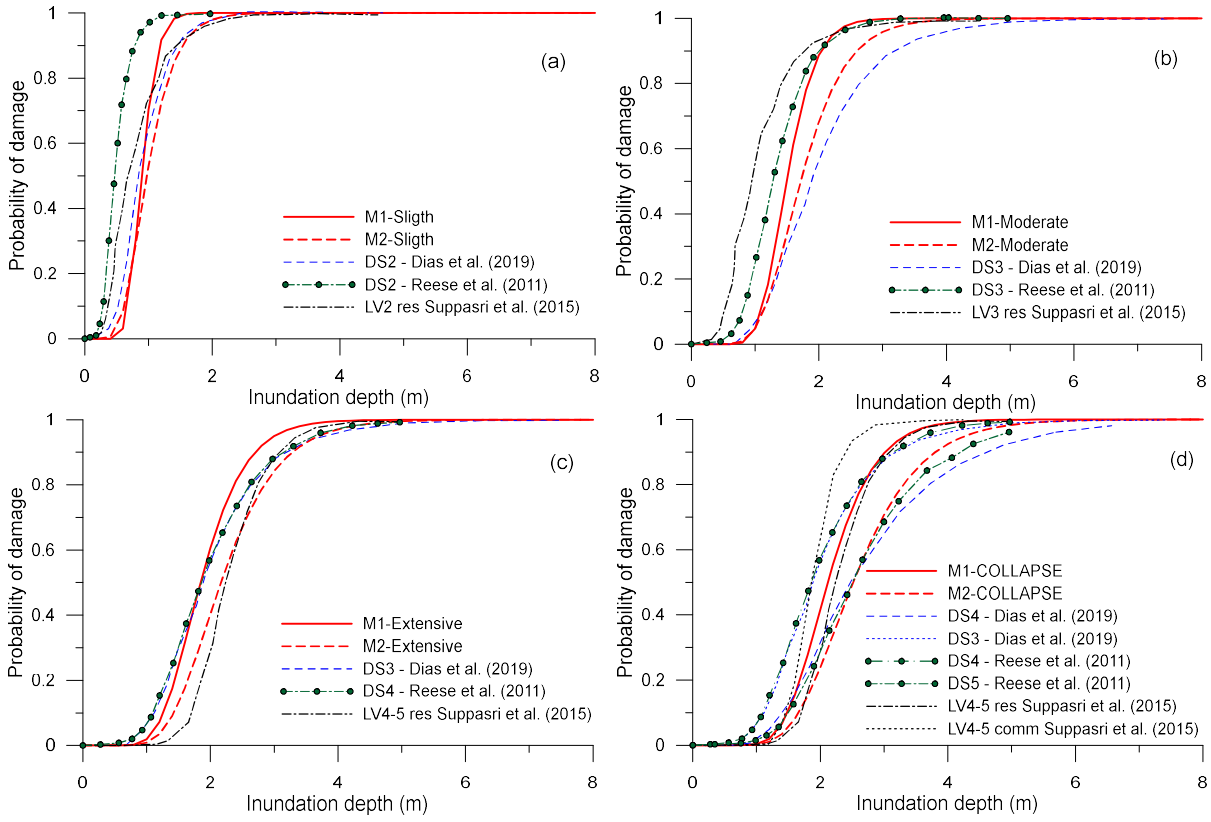

Fig. 12. Analytical (proposed) versus empirical fragility curves at different damage states

5. Conclusions

In this paper, analytical procedure for the determination of fragility curves for single-storey and multi-storey masonry buildings is presented and discussed assuming as study area a small fishing village of the Mediterranean coast, Marzamemi, Sicily. The proposed procedure is applied to a specific study area but can be generalized for other sites because the definition of tsunami forces is decoupled from specific tsunami hazard inundation scenarios, while the definition of the building typologies is related to the site of interest as well as the mechanical characteristics of the materials. The proposed procedure allows defining the fragility curves at collapse state considering the uncertainties in the

evaluation of the capacity and the demand and relates the intermediate damage state as a percentage of the capacity at collapse. The results are in agreement with empirical fragility curves available in the state of the art.

References

Alam, M.S., Barbosa, A.R., Scott, M.H., Cox, D.T., van de Lindt, J.W. (2018). Development of Physics-Based Tsunami Fragility Functions Considering Structural Member Failures. Journal of Structural Engineering. DOI: 10.1061/(ASCE)ST.1943-541X.0001953.

ASCE/SEI 7-16 (American Society of Civil Engineers). (2017). Minimum Design Loads for Buildings and Other Structures, Reston, Virginia.

Asteris, P.G., Moropoulou, A. Skentou, A.D., Apostolopoulou, M., Mohebkhah, A., Cavaleri, L., Rodrigues, H. Varum, H. Stochastic Vulnerability Assessment of Masonry Structures: Concepts, Modeling and Restoration Aspects. Appl. Sci. 2019, 9(2), 243; https://doi.org/10.3390/app9020243.

Benfratello, S., Cavaleri, L., Papia, M. Identification of stiffness, dissipation and input parameters of multi degree of freedom civil systems under unmeasured base excitations. Probabilistic Engineering Mechanics, 24 (2009), 190-198.

Cavaleri, L., Di Trapani, F. & Ferrotto, M.F. A new hybrid procedure for the definition of seismic vulnerability in Mediterranean cross-border urban areas. Nat Hazards 86, 517–541 (2017). https://doi.org/10.1007/s11069-016-2646-9.

Cavaleri, L., Papia, M. An output-only stochastic parametric approach for the identification of linear and nonlinear structures under random base excitations: Advances and comparisons. Probabilistic Engineering Mechanics, 35, 2014, 11-21, https://doi.org/10.1016/j.probengmech.2013.10.010.

461 Charvet I., Macabuag, J., Rossetto, T. (2017). Estimating Tsunami-Induced Building Damage
462 through Fragility Functions: Critical Review and Research Needs. Front. Built Environ. 3:36.doi:
463 10.3389/fbuil.2017.00036.

464 Circolare 21.01.2019, n. 7 C.S.LL.PP: Istruzioni per l'applicazione dell'«Aggiornamento delle
465 "Norme tecniche per le costruzioni"» di cui al decreto ministeriale 17 gennaio 2018., Rome, Italy. (in
466 Italian)

467 D.M. - 17.01.2018: Aggiornamento delle «Norme tecniche per le costruzioni», Rome, Italy. (in
468 Italian).

469 FEMA. Guidelines for the design of structures for vertical evacuation from tsunamis. Washington,
470 D.C.: FEMA P646 prepared by Applied Technology Council for Federal Emergency Management
471 Agency; 2008.

472 Foster A.S.J., Rossetto T., Allsop W. (2017). An experimentally validated approach for evaluating
473 tsunami inundation forces on rectangular buildings. Coastal Engineering 128, 44–57.

474 Foytong, P., Ruangrassamee, A., Lukkunaprasit, P., Thanasisathit, N. Behaviours of reinforced-
475 concrete building under tsunami loading. The IES Journal Part A: Civil & Structural Engineering,
476 2015. http://dx.doi.org/10.1080/19373260.2015.1013998.

477 Ioannou I, Douglas J, Rossetto T (2015) Assessing the impact of ground-motion variability and
478 uncertainty on empirical fragility curves. Soil Dyn Earthq Eng 69:83–92.

479 Karafagka, S, Fotopoulou S, Pitilakis K (2018). Analytical tsunami fragility curves for seaport RC
480 buildings and steel light frame warehouses. Soil Dynamics and Earthquake Engineering 112, 118–
481 137.

482 Pitilakis K., Argyroudis, S., Fotopoulou, S., Karafagka, S, Kakderi, K., Selva, J. Application of stress
483 test concepts for port infrastructures against natural hazards. The case of Thessaloniki port in Greece.
484 Reliability Engineering and System Safety 184 (2019) 240–257.

485 Lagomarsino S, Giovinazzi S (2006) Macroseismic and mechanical models for the vulnerability and
486 damage assessment of current buildings. Bull Earthq Eng 4:415–443.

487 Macabuag J, Raby A, Pomonis A et al. (2018). Tsunami design procedures for engineered buildings:
488 a critical review. Proceedings of the Institution of Civil Engineers – Civil Engineering 171(4): 166–
489 178, https://doi.org/10.1680/jcien.17.00043.

490 Macabuag, J., Rossetto, T., Ioannou, I. et al. (2016). A proposed methodology for deriving tsunami
491 fragility functions for buildings using optimum intensity measures. Nat Hazards. 84: 1257.
492 https://doi.org/10.1007/s11069-016-2485-8.

493 Medina, S., Lizarazo-Marriaga, J., Estrada, M., Koshimura, S., Mas, E., Adriano, B., 2019. Tsunami
494 analytical fragility curves for the Colombian Pacific coast: A reinforced concrete building example.
495 Engineering Structures, 196, 109309.

496 Ministry of Land, Infrastructure, and Transportation (MLIT), 2012. Survey of Tsunami Damage
497 condition, http://www.mlit.go.jp/toshi/toshi-hukkou-arkaibu.html.

498 National Institute of Building Sciences. Direct physical damage-general building stock. HAZUS-MH
499 Technical manual, Chapter 5. Washington, D.C.: Federal Emergency Management Agency; 2004.

500 Petrone, C., Rossetto, T., Goda, K. (2017). Fragility assessment of RC structure under tsunami action
501 via nonlinear static and dynamic analysis. Engineering Structures, 136:36-53.

502 Qi ZX, Eames I, Johnson ER. Force acting on a square cylinder fixed in a free-surface channel flow.
503 J Fluid Mech 2014;756:716–27.

504 Reese, S., Bradley, B.A., Bind, J., Smart, G., Power, W., Sturman, J., 2011. Empirical building
505 fragilities from observed damage in the 2009South Pacific tsunami, Earth-Science Reviews, 107, (1–
506 2):156-173. https://doi.org/10.1016/j.earscirev.2011.01.009

507 Robertson, I. N., K. Pacskowski, H. R. Riggs, and A. Mohamed. 2013. “Experimental Investigation
508 of Tsunami Bore Forces on Vertical Walls.” Journal of Offshore Mechanics and Arctic Engineering
509 135 (2): 021601.1–8. doi:10.1115/ 1.4023149.

510 Rubin, C. M., Horton, B. P., Sieh, K., Pilarczyk, J. E., Daly, P., Ismail, N. & Parnell A.C. Highly
511 variable recurrence of tsunamis in the 7,400 years before the 2004 Indian Ocean tsunami. Nat
512 Commun 8, 16019 (2017). https://doi.org/10.1038/ncomms16019.

513 Shafiei S, Melville BW, Shamseldin AY. Experimental investigation of tsunami bore impact force
514 and pressure on a square prism. Coastal Engineering 110 (2016) 1–16.

515 Silva V, Crowley H, Varum H, Pinho R, Sousa R (2014) Evaluation of analytical methodologies used
516 to derive vulnerability functions. Earthq Eng Struct Dyn 43:181–204.

517 Suppasri A, Charvet I, Imai K, Imamura F. Fragility curves based on data from the 2011 Tohoku-Oki
518 tsunami in Ishinomaki city, with discussion of parameters influencing building damage. Earthq
519 Spectra 2015;31(2):841–68.

520 Suppasri A, Mas E, Charvet I, Gunasekera R, Imai K, Fukutani Y, et al. Building damage
521 characteristics based on surveyed data and fragility curves of the 2011 Great East Japan tsunami. Nat
522 Hazards 2013;66:319–41. http://dx.doi.org/10.1007/s11069-012-0487-8.

523 Suppasri, A., Mas, E., Koshimura, S., Imai, K., Harada, K., and Imamura, F. (2012). Developing
524 Tsunami Fragility Curves From the Surveyed Data of the 2011 Great East Japan Tsunami in Sendai
525 and Ishinomaki Plains, Coast. Eng. J., 54, 1–16, https://doi.org/10.1142/S0578563412500088.

526 Triatmadja, R., Nurhasanah, A. Tsunami force on buildings with openings and protection. Journal of
527 Earthquake and Tsunami Vol. 6, No. 4 (2012) 1250024. (17 pages). DOI:
528 10.1142/S1793431112500248.

529 Tsunami risk assessment and mitigation for the Indian Ocean; knowing your tsunami risk – and what
530 to do about it. IOC Manuals and Guides No. 52, Paris: UNESCO, Second edition 2015 (English).

Valencia, N., Gardi, A., Gauraz, A., Leone, F., Guillande, R. New tsunami damage functions developed in the framework of SCHEMA project: application to European-Mediterranean coasts Nat. Hazards Earth Syst. Sci., 11, 2835–2846, 2011.

Wüthrich D, Pfister M, Nistor I, Schleiss A.J. (2018a). Experimental study on the hydrodynamic impact of tsunami-like waves against impervious freestanding buildings. Coastal Engineering Journal, 60:2, 180-199, DOI:10.1080/21664250.2018.1466676.

Wüthrich D, Pfister M, Nistor I, Schleiss A.J. (2018b). Experimental Study of Tsunami-Like Waves Generated with a Vertical Release Technique on Dry and Wet Beds. Journal of Waterway, Port, Coastal, and Ocean Engineering, ASCE, DOI: 10.1061/(ASCE)WW.1943-5460.0000447.

Wüthrich D, Pfister M, Nistor I, Schleiss A.J. (2018c). Experimental study on forces exerted on buildings with openings due to extreme hydrodynamic events. Coastal Engineering, 140, 72–86.